Transceive Phase Corrected Contrast Source Inversion-Electrical Properties Tomography

Peter R.S. Stijnman[1], Stefano Mandija[1], Patrick S. Fuchs[2], Rob F. Remis[2], and Cornelis A.T. van den Berg[1]

[1]Center for Image Sciences, UMC Utrecht, Utrecht, Netherlands, [2]Circuits and Systems Group, Delft University of Technology, Delft, Delft, Netherlands

Synopsis

Contrast Source Inversion Electrical Properties Tomography (CSI-EPT) is an integral-based method that aims to reconstruct tissue electrical properties through an iterative minimization procedure. This method requires complex B_1^+ data as input. In practice, however, the transmit phase cannot be measured in MRI-experiments. Only the transceive phase can be calculated from MR-measurements. In this work, the CSI-EPT reconstruction algorithm is reformulated to take the transceive phase into account. This transceive phase correction opens the possibility to exploit higher sensitivity of EPT at higher field strengths with regular quadrature setups. Additionally, for the first time CSI-EPT reconstructions from MR-measurements are shown.

Introduction

Helmholtz-based MR-Electrical-Properties-Tomography (MR-EPT) is a derivative-based approach that reconstructs tissue electrical properties (EPs: conductivity σ, permittivity ε) directly from MR-measurements. MR-EPT reconstructions are highly sensitive to noise and present severe boundary artifacts[1].

Alternatively, Contrast-Source-Inversion-EPT (CSI-EPT), an integral-based approach, is less sensitive to noise and boundary artifacts[2]. CSI-EPT requires complex B_1^+ data. However, B_1^+ phase measurements are not possible in practice. Here, the standard CSI-EPT algorithm[2] has been reformulated in terms of the accessible transceive phase, and first reconstructions from MR-measurements are presented.

Methods

The original CSI-EPT method attempts to find tissue EPs by minimizing the cost functional[2]

$$F(w_j,\chi) = \eta_S \sum_j ||B_{1,j}^{+;sc} - G_S\{w_j\}||_S^2 + \eta_D \sum_j ||\chi E_j^{inc} - w_j + \chi G_D\{w_j\}||_D^2, \qquad (1)$$

where the contrast source $w_j = \chi E_j$ (with the contrast function $\chi(\mathbf{x}) = \epsilon_r(\mathbf{x}) - 1 + \frac{\sigma(\mathbf{x})}{i\omega\epsilon}$) and E_j the electric field corresponding to the jth antenna setting operating at the Larmor frequency ω), $\eta_{S,D}$ normalization factors, G_S the data operator mapping contrast sources to scattered B_1^+ data, G_D the object operator mapping contrast sources to electric fields, $B_{1,j}^{+;sc} = B_{1,j}^+ - B_{1,j}^{+;inc}$ the scattered B_1^+ field, while E_j^{inc} and $B_{1,j}^{+;inc}$ are the fields in an empty coil, obtainable through simulations or measurements.

The MR-accessible transceive phase is the sum of the transmit/receive phases, ϕ_+/ϕ_-, respectively. To obtain ϕ_+, the transceive-phase-assumption[3] (TPA) is often used:

$$\phi_+ = \phi_- = \frac{\phi_\pm}{2} \qquad (2)$$

This assumption breaks down for increasing field strengths and non-symmetrical objects. Here, the CSI-EPT formalism is rewritten to include the measured transceive phase:

$$F(w_j,\chi,\phi_-) = \eta_S \sum_j |||B_{1,j}^+|e^{i\phi_\pm}e^{-i\phi_-} - G_S^+\{w_j\} - B_1^{+;inc}||_S^2 + \eta_D \sum_j ||\chi E_j^{inc} - w_j + \chi G_D\{w_j\}||_D^2, \qquad (3)$$

where the B_1^+ field is given in polar form, the transmit phase is written in terms of the transceive (known) and receive (unknown) phases (input data are indicated in blue).

Here, the receive phase is iteratively updated using the current estimates of the contrast function and electric field. Specifically, the scattered receive field is computed at each iteration, n, using

$$B_{1,n}^{-,sc} = G_S\{\chi_{n-1}E_n^{RE}\}, \qquad (4)$$

where E_n^{RE}, the electric field during reception, is:

$$E_n^{RE} = G_D\{\chi_{n-1}E_n^{RE}\} + E^{inc;RE}. \qquad (5)$$

$E^{inc;RE}$, the incident electric field, is modelled together with $B_1^{-inc,RE}$ for an empty birdcage coil.

First, the impact of TPA on CSI-EPT was investigated using 2D-line source simulations (Matlab), mimicking the center plane of a birdcage coil. The field distributions were computed using the phantom contrast (*Fig.1*) and used as input for CSI-EPT reconstructions. Comparison between the EPs reconstructions from TPA (eq.1) and Transceive-Phase-Corrected (TPC, eq.3) was therefore performed.

Furthermore, the impact of noise and field strength was also investigated with realistic Signal-to-Noise-Ratio (SNR) values[4].

Additionally, 3D-FDTD simulations (Sim4Life, ZMT, CH) were performed modeling a 68 cm 3T birdcage coil. Finally, comparison between CSI-EPT and MR-EPT conductivity reconstructions was performed.

MR-measurements (3T, Ingenia, Philips, Netherlands) were conducted using the body/head-coils for transmission/reception, respectively. The B_1^+ magnitude was measured with an AFI sequence[5]. The transceive phase was computed by combining two Spin-Echo sequences with opposite readout polarities[3], and by compensating for the head coil receive sensitivity using an available vendor specific algorithm (CLEAR).

Results & Discussion

Figure 2 shows ϕ_+ and $\frac{\phi_\pm}{2}$ from simulations, measurements and reconstructions. The reconstructed ϕ_+ from MR-measurements resembles well the simulated ϕ_+ even though the transceive phase in the 2D-model has a bigger curvature.

Figure 3 shows the absolute error in conductivity and permittivity reconstructions at 3T and 7T assuming noiseless input data for TPA and TPC. For TPA, the EPs reconstruction error increases with the field strength. If TPC is used, this error is strongly reduced.

Figure 4 shows that the error in CSI-EPT reconstructions is due to noise at low field strengths, whereas it is mainly due to the TPA at higher field strengths. If TPC is used, the reconstruction error decreases with increasing field strength, which is due to the intrinsic increase in SNR and RF field curvature.

Figure 5 shows that MR-EPT reconstructions are highly sensitive to noise (even if high NSA is used), while CSI-EPT reconstructions are more noise-robust. CSI-EPT suffers less from boundary issues compared to MR-EPT. However, CSI-EPT suffers from inaccuracies where the electric field is small (center of the phantom). CSI-EPT permittivity reconstructions (not shown) were not representative, most likely due to a mismatch between the modeled incident fields and the incident fields in the MR-experiment. This mismatch can be considered a systematic error to be further investigated.

Conclusion

In this work, the CSI-EPT algorithm has been reformulated to avoid the need of the transceive phase assumption, opening the way for EPT reconstructions at ultra-high frequencies with a standard birdcage coil setup. Additionally, for the first time CSI-EPT reconstructions from MR-measurements were presented, demonstrating more noise-robustness and less spatial boundary error propagation compared to MR-EPT reconstructions. Still, further investigation to obtain more reliable incident fields and 2D model is required for CSI-EPT.

Acknowledgements

No acknowledgement found.

References

[1] S. Mandija, A.Sbrizzi, P.R. Luijten, and C.A.T. van den Berg, “Error analysis of Helmholtz-based MR-Electrical Pproperty Tomography”, Magnetic Resonance in Medicine,2017;early view. doi:10.10002/mrm.27004.

[2] E. Balidemaj, C.A.T. van den Berg, J. Trinks, A.L.H.M.W. van Lier, A.J. Nederveen, L.J.A. Stalpers, H.Crezee, and R.F. Remis, “CSI-EPT: A Contrast Source Inversion Approach for Improved MRI-Based Electric Properties Tomography,” IEEE Transactions on Medical Imaging,2015;1788–1796.

[3] A.L.H.M.W. van Lier, D.O. Brunner, K.P. Pruessmann, D.W.J. Klomp, P.R. Luijten, J.J.W. Lagendijk, and C.A.T. van den Berg, “B1+ phase mapping at 7 T and its application for in vivo electrical conductivity mapping,” Magnetic Resonance in Medicine,2012; 552–561.

[4] C.M. Collins and M.B. Smith, “Signal-to-noise ratio and absorbed power as functions of main magnetic field strength, and definition of rf pulse for the head in the birdcage coil”, Magnetic Resonance in Medicine,2001;684–691. doi:10.1002/mrm.1091.

[5] V.L. Yarnykh, “Actual flip-angle imaging in the pulsed steady state: A method for rapid three-dimensional mapping of the transmitted radiofrequency field”, Magnetic Resonance in Medicine,2007;192–200.

Figures

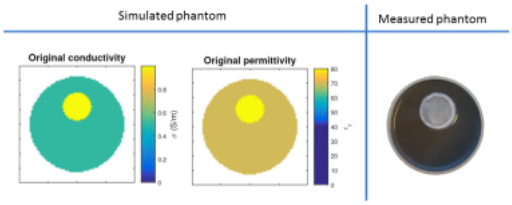

Figure 1: The dielectric properties of the phantom used for the Matlab simulations. Inner compartment: σ = 1 S/m, ε = 80; outer compartment: σ = 0.5 S/m, ε = 70. The phantom has a diameter of 12.8 cm and a length of 15 cm. The inner tube has a diameter of 3.6 cm and a length of 15 cm. The sub-figure on the right shows the agar-based phantom, which had roughly the same dimensions but slightly lower conductivity values (0.95 S/m for the inner tube and 0.45 S/m for the outer compartment).

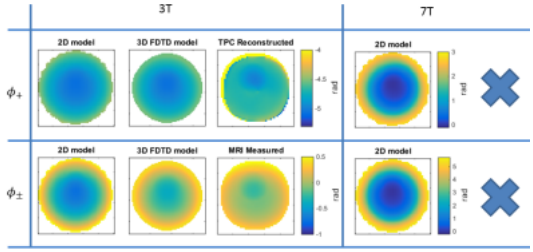

Figure 2: Top row: the transmit phase Φ+. From left to right: the first sub-figure is the simulated Φ+ at 3T (Matlab), the second subfigure is the Φ+ simulated with Sim4Life, the third sub-figure is the reconstructed Φ+ from MR-measurements at 3T, and the fourth sub-figure is the Φ+ simulated at 7T (Matlab). Bottom row: the transceive phase Φ±. From left to right, the same structure as the top row is adopted. However, only Matlab simulations are presented for 7T.

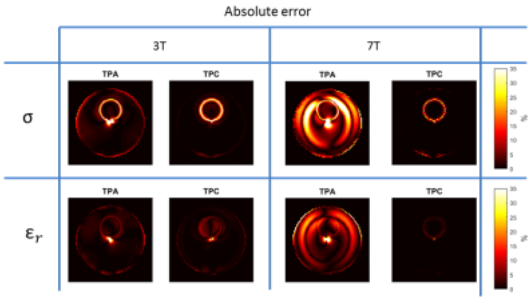

Figure 3: The top row shows the absolute error in the CSI-EPT conductivity reconstruction. The bottom row shows the absolute error in the CSI-EPT permittivity reconstruction. The first column refers to CSI-EPT reconstruction at 3T with the TPA as input data, the second column refers to the CSI-EPT reconstruction at 3T with the reformulated algorithm (TPC). The third and fourth columns are the same as the first two but at 7T.

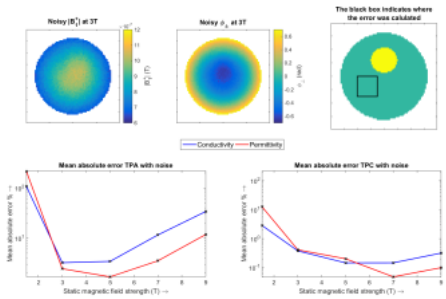

Figure 4: Example of noisy B_1^+ magnitude and transceive phase maps at 3T (top-left, top middle), used in the simulations, are shown. The ROI used to compute mean absolute errors is shown in the top-right sub-figure. The plots in the bottom row show the mean absolute error for different field strengths if TPA (bottom-left) or TPC (bottom-right) is used for noisy input data. Note that for TPC, the error is one order of magnitude lower than TPA.

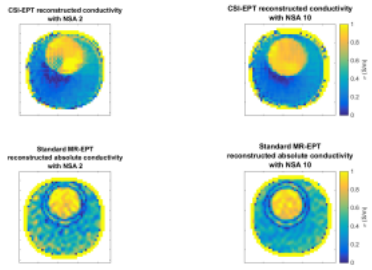

Figure 5: Reconstructed absolute conductivity maps from MR-measurements (voxel size = 2.5 mm, isotropic): CSI-EPT (top row) and MR-EPT (bottom row) using different number-of-signal-averages (NSA: 2 and 10,respectively left and right) are shown. For MR-EPT, a 7×7 voxels finite difference second order derivative kernel was employed. The average conductivity value for the CSI-EPT reconstruction (NSA = 10) is 0.34 S/m (outer compartment) and 0.88 S/m (inner compartment). The average conductivity value for the MR-EPT reconstruction (NSA = 10) is 0.47 S/m (outer compartment) and 0.92 S/m (inner compartment), computed after excluding boundary regions which are affected by numerical errors.